Vibration and Stability Behaviour of Strengthened Thin-Walled Slender RC Columns using CFRP Laminates

T Rajanna [1*], P.K Ravindra[2], G Venkataramaiah[3], S Manjunatha[4] and Imran Khan[5]

[1*] Associate Professor, t.rajanna@gmail.com, B.M.S. College of Engineering, Bengaluru 560019, India

[2] Associate Professor, ravindrapkravindra@ymail.com, Government Engineering College Ramanagara 562159, India

[3] Associate Professor, gvr66ramaiah@gmail.com, Government Engineering College Ramanagara 562159, India

[4] Associate Professor, manjunathswamy67@gmail.com, Government S.K.S.J.T.I, Bengaluru 560001, India

[5] Associate Professor, imrangce@gmail.com, Government Engineering College Ramanagara 562159, India

Abstract: This paper investigates the vibration and buckling behavior of thin-walled, slender reinforced concrete (RC) columns retrofitted with carbon fiber-reinforced polymer (CFRP) laminates. The study addresses the structural performance of such columns under various partial and concentrated edge loading conditions, which are less explored in existing literature. A finite element code developed in MATLAB is employed to perform a comprehensive parametric analysis. The natural frequencies of the columns are evaluated by incorporating key influencing factors, including load eccentricity, column height, boundary conditions, and ply orientation of CFRP laminates. The impact of applied loads on the dynamic characteristics is also examined. Material properties are carefully computed by accounting for both concrete and embedded reinforcement, ensuring realistic modeling. Furthermore, the buckling behavior of retrofitted columns is studied under varying loading and geometric conditions. Results demonstrate that CFRP retrofitting significantly enhances both stiffness and stability, while load eccentricity and slenderness influence vibration modes and critical loads. This study contributes valuable insights toward the design and analysis of slender RC columns in modern construction systems, especially where retrofitting and performance under complex loading are of concern.

***Keywords*:** Buckling, vibration, thin-walled columns, finite element method, FRP retrofitting.

1. Introduction:

In recent years, the focus on strengthening and rehabilitating aging or structurally deficient buildings has intensified within the construction industry [[1], [2]]. To enhance the load-bearing capacity of reinforced concrete (RC) columns under various loading scenarios, a range of strengthening techniques has been developed. Traditional solutions such as concrete jacketing with or without supplemental reinforcement [[3], [4]] along with ferro-cement layers [[5], [6]] and engineered cementatious composites (ECC) [[7], [8]], have proven effective, but often at the cost of increased column dimensions and dead load.

To address these drawbacks, fiber-reinforced polymer (FRP) composites have emerged as a promising alternative. Known for their exceptional strength-to-weight ratio, resistance to corrosion, and ease of installation, FRPs are now widely used in civil engineering applications [[9], [10]]. Over the past two decades, substantial research has confirmed that the application of FRP can significantly improve both the strength and ductility of plain and reinforced concrete elements [[11], [12]]. Given the critical role that columns play in maintaining the structural integrity of buildings, strengthening deficient columns remains a key concern. One widely adopted method involves wrapping columns with FRP, with fibers oriented primarily in the hoop direction to restrict lateral expansion of the concrete core and enhance confinement [[13], [14]]. Numerous studies have validated the efficacy of FRP confinement. Hadi [15], for example, observed that RC columns confined with CFRP exhibited notable improvements in load-carrying capacity, ductility, and moment redistribution. Similarly, Belouar et al. [16] demonstrated that adding more CFRP layers increases compressive strength, although ductility tends to decrease with higher slenderness ratios. From a computational perspective, Charalambidi et al. [17] used finite element models employing 8-noded elements to simulate partial GFRP

confinement in low-strength concrete, while Hales et al. [18] explored the benefits of internal FRP spirals and longitudinal bars, which were shown to substantially enhance tensile strength and overall load resistance.

Due to the absence of comprehensive design guidelines for slender FRP-confined columns, researchers have proposed various theoretical models. Jiang and Teng [19], for instance, introduced a numerical model based on Lam and Teng's stress–strain relationship, achieving results that closely matched experimental outcomes. However, they emphasized the importance of further large-scale testing for validation. In the context of hybrid systems, Chellapandian et al. [20] investigated RC columns retrofitted with both CFRP laminates and external fabrics under axial and eccentric loading. Their experimental, analytical, and finite element evaluations confirmed that hybrid retrofitting significantly enhances initial stiffness, peak load, and ductility, with predictions deviating by less than 5% from actual test results. Similarly, Mosallam [21] studied retrofitted RC beam-column joints using high-strength, high-modulus CFRP laminates and hybrid composite connectors, showing enhanced performance under cyclic and gravity loads. Beyond column confinement, researchers have also focused on the behavior of laminated composite plates. Sahu et al. [22] examined the buckling behavior of plates with various symmetric and anti-symmetric ply orientations, while Nali and Carrera [23] analyzed the mechanical response of orthotropic and anisotropic laminates with different stacking configurations, contributing valuable insights into structural behavior under complex loading.

Despite these advancements, the literature remains limited with respect to slender, thin-walled RC columns especially those retrofitted with FRP and subjected to eccentric or edge loads. Most prior studies have focused on square or circular columns under concentric loading. As slender columns are frequently used in modern structural systems, understanding their vibration and buckling behavior is crucial. This study aims to bridge that gap by conducting a detailed parametric investigation into the effects of FRP confinement, ply orientation, eccentric load application, column height, and boundary conditions. Through this comprehensive assessment, the research seeks to advance the design and retrofitting strategies for slender FRP-retrofitted RC columns under diverse loading conditions.

2. Thin-Walled Slender Columns under Eccentric Loading.

Thin-walled slender columns are structural elements with relatively small cross-sections compared to their length, making them vulnerable to instability under axial and eccentric loads. Unlike stocky columns, their load-carrying capacity is significantly influenced by slenderness ratio rather than material strength alone. Figures 1(a) and 1(b) highlight the geometric slenderness of these columns. As length increases, their sensitivity to load placement and buckling effects becomes more pronounced, underscoring the need for precise stability assessment in design.

(a) (b)

Fig 1: (a)-(b) Thin walled slender columns

The representative cases of partial in-plane edge loading and concentrated edge loading considered in this study are illustrated in Fig. 2(a)–(d). For each configuration, the total axial load PPP remains constant regardless of the localized load width along the column edge. These loads are compressive and applied over a limited portion of the column's cross-section. In the diagrams, the parameter 'c' denotes the width of the applied load, while 'b' represents the total width of the column. When the ratio c/b = 1, the loading becomes uniform across the column width for the respective cases shown.

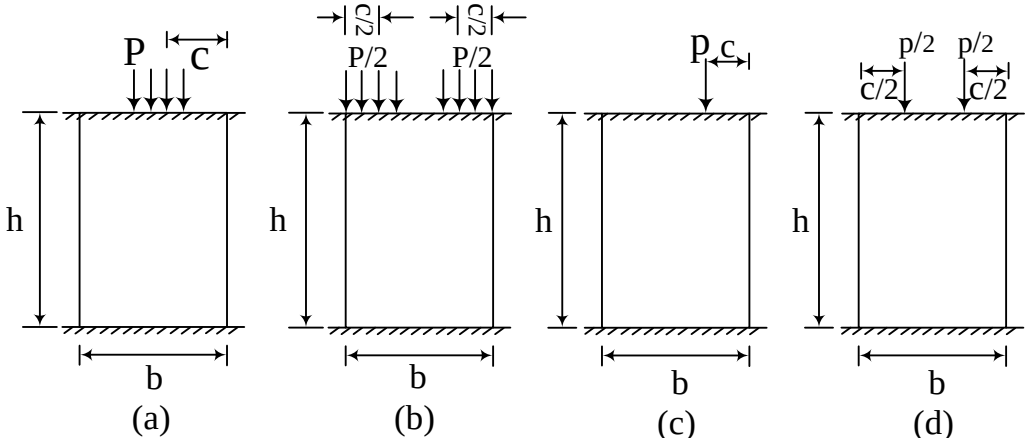

Fig 2: Problem description: Partial edge loading (a) from one end, (b) from both ends and Point load (c) from one end, (d) from both ends.

3. Finite element formulation and governing equations

A typical plate, as illustrated in Fig. 3, has dimensions a × b × h along the x, y, and z axes, respectively. The plate is composed of a unidirectional composite fiber laminate. To derive the expression for strain energy, five independent displacement coordinates are considered: u, v, and w, representing displacements along the x, y, and z directions, and Θ_x and Θ_y, representing rotations about the y and x axes, respectively. These displacement components form the basis for analyzing the plate's deformation behavior under loading.

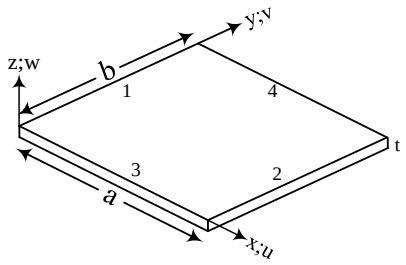

Fig 3: Lamina geometry of plate

The First-order Shear Deformation Theory (FSDT) is employed, incorporating a shear correction factor to account for the non-linear shear strain distribution through the thickness. The displacement field assumes that normals to the mid-surface remain straight but not necessarily perpendicular after deformation, such that

$$\left\{\bar{u}^p(x,y,z),\ \bar{v}^p(x,y,z),\ \bar{w}^p(x,y,z)\right\} = \left\{u^p(x,y),\ v^p(x,y),\ w^p(x,y)\right\} + z\left\{\theta_x^p(x,y),\ \theta_y^p(x,y),\ 0\right\} \quad (1)$$

where $\bar{u}^p$,$\bar{v}^{pi}$and $\bar{w}^p$represent the displacements in the x, y, and z directions,while u^p, v^p, and w^pdenotemid-plane displacements along x, y, and z axes. Additionally,θ_x^p and θ_y^pindicate rotations of the normalto the un-deformed mid-plane of the plate about the y and x-axes, respectively. In the current formulation, Eq. (2) presents the Green-Lagrange's strain displacement relation for a plate element.

$$\left.\begin{aligned}
\varepsilon_{xp} &= \left(\frac{\partial \overline{u}^{p}}{\partial x}\right)+\frac{1}{2}\left(\frac{\partial u^{p}}{\partial x}\right)^{2}+\frac{1}{2}\left(\frac{\partial v^{p}}{\partial x}\right)^{2}+\frac{1}{2}\left(\frac{\partial w^{p}}{\partial x}\right)^{2}+\frac{1}{2}z^{2}\left[\left(\frac{\partial \theta_{x}^{p}}{\partial x}\right)^{2}+\left(\frac{\partial \theta_{y}^{p}}{\partial x}\right)^{2}\right] \\
\varepsilon_{yp} &= \left(\frac{\partial \overline{v}^{p}}{\partial y}\right)+\frac{1}{2}\left(\frac{\partial u^{p}}{\partial y}\right)^{2}+\frac{1}{2}\left(\frac{\partial v^{p}}{\partial y}\right)^{2}+\frac{1}{2}\left(\frac{\partial w^{p}}{\partial y}\right)^{2}+\frac{1}{2}z^{2}\left[\left(\frac{\partial \theta_{x}^{p}}{\partial y}\right)^{2}+\left(\frac{\partial \theta_{y}^{p}}{\partial y}\right)^{2}\right] \\
\gamma_{xyp} &= \left(\frac{\partial \overline{u}^{p}}{\partial y}+\frac{\partial \overline{v}^{p}}{\partial x}\right)+\frac{\partial u^{p}}{\partial x}\frac{\partial u^{p}}{\partial y}+\frac{\partial v^{p}}{\partial x}\frac{\partial v^{p}}{\partial y}+\left(\frac{\partial w^{p}}{\partial x}\right)\left(\frac{\partial w^{p}}{\partial y}\right)+z^{2}\left[\frac{\partial \theta_{x}^{p}}{\partial x}\frac{\partial \theta_{x}^{p}}{\partial y}+\frac{\partial \theta_{y}^{p}}{\partial x}\frac{\partial \theta_{y}^{p}}{\partial y}\right]
\end{aligned}\right\} \quad (2)$$

The strain-displacement equation, which is shown in Eq. (2) has two parts, i.e., linear strain and non-linear strains,

$$\left\{\varepsilon_{ij}\right\} = \left\{\varepsilon_{ij}^{L}\right\} + \left\{\varepsilon_{ij}^{NL}\right\} \quad (3)$$

The linear strain vector $\{\varepsilon_{ij}^{L}\}$ is employed for the elastic stiffness matrix, and the non-linear strain term $\{\varepsilon_{ij}^{NL}\}$ is used for the geometric stiffness matrix. Under the assumption of minimal and neglected normal stresses, the stress-strain relation for the laminated panel is derived based on the displacement model as,

$$\begin{Bmatrix} N_x^p \\ N_y^p \\ N_{xy}^p \\ M_x^p \\ M_y^p \\ M_{xy}^p \\ Q_{xz}^p \\ Q_{yz}^p \end{Bmatrix} = \begin{bmatrix} A_{11}^p & A_{12}^p & A_{16}^p & B_{11}^p & B_{12}^p & B_{16}^p & 0 & 0 \\ A_{12}^p & A_{22}^p & A_{26}^p & B_{12}^p & B_{22}^p & B_{26}^p & 0 & 0 \\ A_{16}^p & A_{26}^p & A_{66}^p & B_{16}^p & B_{26}^p & B_{66}^p & 0 & 0 \\ B_{11}^p & B_{12}^p & B_{16}^p & D_{11}^p & D_{12}^p & D_{16}^p & 0 & 0 \\ B_{12}^p & B_{22}^p & B_{26}^p & D_{12}^p & D_{22}^p & D_{26}^p & 0 & 0 \\ B_{16}^p & B_{26}^p & B_{66}^p & D_{16}^p & D_{26}^p & D_{66}^p & 0 & 0 \\ 0 & 0 & 0 & 0 & 0 & 0 & S_{44}^p & S_{45}^p \\ 0 & 0 & 0 & 0 & 0 & 0 & S_{45}^p & S_{55}^p \end{bmatrix} \begin{Bmatrix} u_{,x}^p \\ v_{,y}^p \\ u_{,y}^p + v_{,x}^p \\ \theta_{x,x}^p \\ \theta_{y,y}^p \\ \theta_{x,y}^p + \theta_{y,x}^p \\ w_{,x}^p + \theta_{\mathrm{xp}} \\ w_{,y}^p + \theta_{\mathrm{yp}} \end{Bmatrix} \quad (4)$$

where the comma subscriptdenotes differentiation with respect to the coordinates following the subscript.

The laminates constitutive coefficients in Eq. (7) are defined by,

$$(A_{ij}^P,\ B_{ij}^P,\ D_{ij}^P) = \sum_{k=1}^{m}\int_{z_{k-1}}^{z_k}\left(\overline{Q}_{ij}^p\right)(1,\ z,\ z^2)\ dz \quad \text{for i, j= 1, 2, 6} \quad (5)$$

whereas the shear component is indicated by $S_{ij}^P = \sum_{k=1}^{m}\int_{z_{k-1}}^{z_k}\kappa^p\left(\overline{Q}_{ij}^p\right)dz$ for i, j= 4,5 (6)

Here κ^p is the shear correction factor, which is used to compensate for the parabolic shear stress distribution across the plate thickness and is taken to be 5/6.

The linear and non-linear strain terms in Eq (2) and resultant stress-strain relations in Eq. (4) are used to derive the different level stiffness matrices as follows:

$$\left[k_e^p\right] = \int_{-1}^{1}\int_{-1}^{1}\left[B^p\right]^T\left[D^P\right]\left[B^p\right]\left|J^p\right|d\xi d\eta \quad (7)$$

$$\left[k_G^p\right] = \int_{-1}^{1}\int_{-1}^{1}\left[B_G^p\right]^T\left[S^P\right]\left[B_G^p\right]\left|J^p\right|d\xi d\eta \quad (8)$$

$$\left[m^p\right] = \int_{-1}^{+1}\int_{-1}^{+1}\left[\overline{N}^p\right]^T\left[\overline{I}^p\right]\left[\overline{N}^p\right]\left|J^p\right|d\xi d\eta \quad (9)$$

where $\left[k_e^p\right]$, $\left[k_G^p\right]$ and $\left[m^p\right]$ represents element level stiffness, geometric stiffness and mass matrices, respectively. Structural stiffness matrices are assembled from individual element-level matrices using the skyline technique. The complete FE formulation, including different stiffness matrices for the heterosis element in this study is referenced from the work of Rajannaet al. [20] and is not discussed here for brevity.

The governing differential equation of equilibrium for a structural component under the application of in-plane edge load can be obtained by using extended Hamilton's principle as,

$$\left[\mathrm{M}\right]\{\ddot{\mathrm{q}}\} + \left[\left[\mathrm{K}\right] - \mathrm{P}_0\left[\mathrm{K}_\mathrm{G}\right]\right]\{\mathrm{q}\} = \{0\} \quad (10)$$

The assembled matrices [K], [K_G], and [M] represent system elastic stiffness, geometric stiffness, and mass, respectively. Equation (10) can be simplified for buckling and vibration scenarios.

In the case of buckling, when$\{\ddot{q}\}$=0, the equationreduces to:

$$\left[\mathrm{K}\right]\{\mathrm{q}\} - \mathrm{P}_{\mathrm{cr}}\left[\mathrm{K}_\mathrm{G}\right]\{\mathrm{q}\} = \{0\} \quad (11)$$

In the case of vibration, equation (10) becomes,

$$\left[\mathrm{K}\right]\{\mathrm{q}\} - \mathrm{P}_0\left[\mathrm{K}_\mathrm{G}\right]\{\mathrm{q}\} - \omega^2\left[\mathrm{M}\right]\{\mathrm{q}\} = \{0\}. \quad (12)$$

In Eq. (12), when P_0 approaches zero, the equationdescribes free vibration without in-plane load, while the presence of P_0 signifies a vibration problem with in-plane load effects. Setting ω^2 to zero in Eq. (12) for a specific P_0 value identifies the critical buckling load. This dynamic approach to determine critical loads is advantageous as it circumvents singularity issues posed by eigen value solvers in static analysis. This method has been applied to ascertain critical loads for diverse problems in the study.

4. PROBLEM DESCRIPTION

This study investigates the buckling and vibration behavior of retrofitted thin-walled RC columns subjected to various in-plane edge loading scenarios, as illustrated in Fig. 2. Key parameters such as stress–strain relations, engineering

constants, and failure criteria for angle-ply laminates are established for analysis. Unlike isotropic materials, composite properties depend on multiple factors—fiber and matrix characteristics, volume fraction, geometry, and manufacturing process—making experimental determination complex and costly. When material symmetry aligns with the fiber direction, five independent elastic constants are required to define the lamina's elastic response.
Several analytical models exist to estimate these constants based on micromechanical relations between the matrix and fiber, as detailed in the works of Whitney and Riley [26], Halpin and Tsai [27], Selvadurai and Nikopour [28], and Hashin and Rosen [29].

4.1 governing elastic properties of the composite material.

The rule of mixture is known as Voigt model, while the Reuss model is renowned as the inverse rule of mixture. Rule of mixture is a simple relationship or approach to approximate longitudinal and transverse direction of the composite material characteristics and these relations are mentioned below,

a) Longitudinal direction (E_1) (12)

$$E_{11} = [(E_S * V_S) + (E_C * V_C)]$$

b) Transverse direction (E_2) (13)

$$\frac{1}{E_{22}} = \frac{V_S}{E_S} + \frac{V_C}{E_C}$$

c) Rigidity Modulus (G) (14)

$$\frac{1}{G_{12}} = \frac{V_S}{G_{S1}} + \frac{V_C}{G_C} G_{23} = \frac{E_{22}}{2 * (1 + \gamma_{23})}$$

Where,

E_S= Young's Modulus of reinforcement steel

E_c= Young's Modulus of Cement concrete

V_S = Volume of Steel

V_c = Volume of Concrete.

4.1.2 Semi Empirical Models

Semi-empirical modelling is a generic word for operations that by observation and experimentation generate models. Semi-empirical modelling relates to a specific range of empirical relationships in which models are built on specific principles. Here in this case semi empirical models have been emerged to correct the errors, under this category some of the important models are modifies rule of mixture, the Halpin-Tsai model [27] and Chamis model [30].

i. Modified Rule of Mixture (MROM) equations are as follows.

$$\frac{1}{E_{22}} = \frac{n^s * V^s}{E^s} + \frac{n^c * V^c}{E^c} \quad (15)$$

Where n^s and n^c are correction factors

$$\eta^s = \frac{E^s * V^s + [(1 - \gamma^s * \gamma^s)E^c + \gamma^c \gamma^s * E^s]V^m}{E^s * V^s + E^c * V^c}$$

$$\eta^c = \frac{[E^s * \left(1 - \gamma^{c^2} - (1 - \gamma^c * \gamma^s) * E^c\right] * V^s + E^c * V^c}{E^s * V^s + E^c * V^c} \quad (16)$$

Where V^s = Volume fraction of steel (17)

V^c = Volume fraction of concrete

γ^s = poisson′sratioofsteel

γ^c = poisson′sratioofconcrete

$$\frac{1}{G_{12}} = \frac{\frac{V^s}{G_{12}^s} + \frac{\eta * V^c}{G^c}}{V^s + \eta' * V^c} \text{ with } 0 < \eta' < 1 \text{ [it'spreferred} \eta = 0.6] \quad (18)$$

ii. Halpin and Tsai [27] proposed semi empirical relations for predicting elastic modulus. These relationships have been created by adjusting the curve to the elasticity based outcomes and the equations are as shown below.

$$E_{22} = E^C\left(\frac{1 + \zeta * \eta * V_s}{1 - \eta * V_s}\right) \quad (19)$$

$$G_{12} = E^C\left(\frac{1 + \zeta * \eta * V_s}{1 - \eta * V_s}\right) \quad (20)$$

$\zeta =$ reinforcing factor depending upon diretion of loading (1 and 2 for E and G respectively,

$\eta =$ Stress Participation Factor,

$$\eta = \frac{(E_s/E_c) - 1}{(E_s/E_c) + \zeta} \quad (21)$$

iii. Chamis [30] has proposed equations similar to Halpin and Tsai, for calculating elastic modulus in transverse direction and shear modulus as follows

$$E_{11} = [(E_S * V_S) + (E_C * V_C)] \quad (22)$$

$$E_{22} = \frac{E_c}{1 - \sqrt{V_s} * \left(1 - \frac{E_c}{E_s}\right)} \quad (23)$$

$$\gamma_{12} = (V_s * \gamma_s) + (V_c * \gamma_c) \quad (24)$$

$$G_{12} = \frac{G_c}{1 - \sqrt{V_s} * \left(1 - \frac{G_c}{G_s}\right)} \quad (25)$$

$$G_{23} = \frac{G_c}{1 - \sqrt{V_s} * \left(1 - \frac{G_c}{G_s}\right)} \quad (25)$$

The values of E_{11}, G_{12}, G_{23} and γ_{12} are correlated to experimental data for different V_s values, but only when E_{22} correlates with experimental data the volume of fiber is greater than or equal to 30% or 0.3 as specified.

4.1.3 Elasticity Approach Model

There are also expressions for elastic moduli based on elasticity in relation to the strength of materials and semi-empirical equation methods. Elasticity approach [19]accounts for Hooke's law relationships in three dimensions, equilibrium of forces and compatibility, the strength of materials approach may not satisfy compatibility and/or account for Hooke's law in three dimensions. The other feasible approach for evaluating the elastic module of a UD lamina is therefore the elasticity method suggested by Hashin & Rosen [29].In this category the models based on composite cylinder assemblage(CCA) model.

$$E_1 = V^s * E^s + E^c * V^c + \frac{4 * V^s * V^c(\gamma^s - \gamma^c)^2}{\frac{V^s}{K^c} + \frac{1}{G^c} + \frac{V^c}{K^s}} \quad (26)$$

$$\gamma_{12} = V^s * \gamma_{12}^s + V^c * \gamma^c \quad (27)$$

$$G_{12} = G^c * \frac{G^s(1+V^s) + G^c * V^c}{G^s * V^c + G^c(1+V^s)} \quad (28)$$

4.1.4 Whitney And Riley Estimates

The elastic constants of a unidirectional fiber-reinforced elastic matrix were estimated by Whitney and Riley [26]. These developments are based on the representative elements ' structural mechanics models and are less strict than the processes established by Hashin and Rosen and others based on elasticity variation theorems, the equations are discussed below.

$$E_{11} = \left[\left((E_s - E_c) * V_S\right) + (E_C * V_C)\right] \quad (29)$$

$$G_{23} = \frac{[(G_s + G_c) + (G_s - G_c) * G_c V_s]}{[(G_s + G_c) - (G_s - G_c) * V_s]} \quad (30)$$

$$\gamma_{12} = \gamma_c - \frac{2 * (\gamma_c - \gamma_s)(1-\gamma_c)^2 * E_s * V_s}{E_c(1-V_s)L_1 + E_s\left(V_s L_2 + (1+\gamma_c)\right)} \quad (31)$$

$$\gamma_{23} = (V_s * \gamma_s) + (V_c * \gamma_c) \quad (32)$$

where, $L_1 = 1 - \gamma_s - {\gamma_s}^2$ and $L_2 = 1 - \gamma_c - {\gamma_c}^2$ (33)

Isotropic properties of concrete and steel are noted as in table 1. The values mentioned in Table. 2 where validated with the help of 'Autodesk Helius Composite 2016' and the values obtained are in Psi units. Based on the comparison with Phenomenological Models and software it was concluded that the values were approximately equal or near to the valued that were obtained from software.

Table 1: Isotropic properties of concrete and steel

Particulars		Concrete
Young's modulus	E_c	25000 MPa
Shear modulus	G_c	10869.5 MPa
Poisson's value	ϑ_c	0.15
Density	ρ_c	2400 Kg/m^3

Particulars		Steel
Young's modulus	E_s	200000 MPa
Shear modulus	G_s	76869.5 MPa
Poisson's value	ϑ_s	0.30
Density	ρ_s	7850 Kg/m^3

Table 2: Calculated concrete equivalent young's modulus for varying % of steel

Sl. No	Particulars	Percentage of steel (Volume fraction Vs)				
		0.8	1	2	2.5	3
1.	**Longitudinal Direction(E_{11}) (N/mm^2)**					
a.	Rule of mixture	26400.00	26750.00	28500.00	29375.00	30250.00
b.	MROM	26400.00	26750.00	28500.00	29375.00	30250.00
c.	Chamis method [30]	26400.00	26750.00	28500.00	29375.00	30250.00
d.	Elasticity approach	26407.10	26759.11	28517.93	29397.23	30276.40

2.	**Transverse Direction(E_{22}) (N/mm^2)**					
a.	Inverse rule of mixture	25176.20	25220.60	25445.90	25559.11	25673.90
b.	MROM	25338.80	25421.93	25829.46	26028.80	26225.60
c.	Chamis method [30]	31377.90	31746.03	33277.59	33937.40	34556.80
d.	Halpin– Tsai [27]	25201.10	25252.53	25510.20	25641.03	25773.20
3.	**Rigidity Shear Modulus (G_{12}= G_{13} and G_{23}) (N/mm^2)**					
a.	Rule of mixture	10944.70	10963.71	11059.50	11108.03	11156.90
b.	MROM	10994.70	11026.32	11185.52	11266.04	11347.20
c.	Chamis method 30]	13901.60	14064.70	14743.24	15035.56	15310.00
d.	Elasticity approach	11001.20	11034.37	11201.68	11286.31	11371.80
e.	Rule of mixture (G_{23})	11005.30	11038.61	11200.98	11280.08	11358.00
4.	**poisson's ratios (ϑ_{12})**					
a.	Rule of mixture	0.1512	0.1515	0.153	0.1537	0.1545
b.	elasticity approach	0.1519	0.1523	0.1547	0.1559	0.1571

The above mentioned Table. 2 provided values of young's modulus of RCC by assigning the properties of concrete and steel specifically, for different percentage of steel varying from 0.8% to 3.0%.

Table 3: Geometric boundary conditions

Boundary condition		Position of the edge	
		y = 0 (bottom)	y = b (top)
Simply supported (S)		x = 0, w = 0, $\theta_y = 0$	w = 0, $\theta_y = 0$
Clamped (C)	BC-1	x = 0, y = 0, w = 0, $\theta_x = 0$, $\theta_y = 0$	x = 0, w = 0, $\theta_x = 0$, $\theta_y = 0$
	BC-2	x = 0, y = 0, w = 0, $\theta_x = 0$, $\theta_y = 0$	x = 0, $\theta_x = 0$, $\theta_y = 0$
Free (F)		No restraints	

The present investigation in mainly focused on the slender concrete column with retrofitting. First the isotropic properties of concrete and steel are used to calculate the orthotropic properties of the RCC by considering it as composite material and the properties of the retrofitting material is selected from Kishore et al. [25] based on the comparison with experimental data and the results. As mentioned in table 4.

Table 4: Material properties of slender column for 2% steel and epoxy/carbon laminate.

Material	Material constants					
	E_{11}	E_{12}	G_{12}	G_{13}	G_{23}	ν_{12}
RC Column	28.54e3	25.82e3	11.20e3	11.20e3	11.20e3	0.153
Carbon/epoxy	172.5e3	6.9e3	3.5e3	3.5e3	1.4e3	0.25

5. RESULTS AND DISCUSSIONS

Convergence studies

Accurate discretization is essential in finite element analysis to ensure reliable convergence. In this study, the column is modeled using a mesh of m×n times ements, representing rows and columns respectively. The applied loading, as shown in Fig. 2, is compressive in nature, with a localized load width ratio of c/b =0.5. A mesh size of 20×10 yielded satisfactory convergence, as shown in Table 5, and is therefore adopted consistently throughout the analysis.

Table 5: Convergence of buckling load (γ_{cr}) for CC edge partial load for c/b = 0.5

Mesh order, m x n	$[\pm0]_s$/RCC/$[\pm0]_s$	$[\pm90]_s$/RCC/$[\pm90]_s$
4 x 2	3.775 x 10^4	5.332 x 10^4
8 x 4	3.764 x 10^4	5.236 x 10^4
12 x 6	3.695 x 10^4	5.165 x 10^4
16 x 8	3.601 x 10^4	5.095 x 10^4
20 x 10	3.512 x 10^4	5.068 x 10^4
24 x 12	3.512 x 10^4	5.068 x 10^4

Comparison studies

Comparison studies are essential to evaluate the accuracy and reliability of different matrix formulations and discretization techniques used in vibration and buckling analysis. To validate the developed finite element model, the natural frequencies and mode shapes of a square laminated plate were computed using an 8-noded serendipity element (8-NSE). These results were then compared with the closed-form solutions reported by Sahu et al. [22] (Table 6) and Nali & Carrera [23] (Table 7), demonstrating good agreement.

Table 6: Non-dimensional buckling load comparison for simply supported loads between current finite element methods.($W = P_{cr}*b^2 / E_{22}*h^3$) a/b = 1, E_{11}/E_{22} = 25, $G_{12} = G_{13} = 0.5E_{22}$, $G_{23} = 0.1E_{22}$ and v_{12} = 0.25.

C/b ratio	Particulars	Ply-orientation [θ/- θ/ θ/- θ]					
		0	15	30	45	60	90
0.2	Sahu et al. [22]	70.5	73.4	76.6	35.25	19.65	14.91
	Present values	70.13	73.05	76.41	35.01	19.58	14.77
0.6	Sahu et al. [22]	34.68	39.98	49.76	35.25	25.78	13.01
	Present values	33.68	39.63	49.04	35.03	25.52	12.84
1.0	Sahu et al. [22]	23.37	25.21	32.03	35.78	29.59	10.45
	Present values	23.07	24.97	31.84	35.21	29.16	10.22

Table 7: Non-dimensional buckling load comparison for simply supported loads between current finite element methods;E_1/E_2 = 30, G_{12}/E_2 = G_{13}/E_2 = 0.5, G_{23}/E_2 = 0.2, v_{12} = 0.3.

E_1/E_2	Nali& Carrera [23]	D'Ottavio and Carrera	Present values
3	5.533	5.399	5.539
10	10.249	9.965	11.244
20	15.798	15.351	16.401
30	20.306	19.756	22.525
40	24.051	24.429	26.551

The simply supported square plate is analysed and non-dimensional natural frequency is determined using present method and compared with the research paper of Tseng and Chou [24] and represented in Table 8.

Table 8: Non-dimensional fundamental frequency comparison for simply supported between current finite element methods; G_{12}/E_{22} = G_{13}/E_2 = 0.6, G_{23}/E_{22} = 0.5, v_{12} = 0.25 $\left(\bar{\omega} = \omega a^2 \sqrt{\frac{\rho}{Eh^2}}\right)$

E_1/E_2	[0/90/90/0]			[0/90/0/90]		
	Noor	Tseng [24]	Present values	Noor	Tseng [24]	Present values
3	0.264	0.263	0.262	0.261	0.259	0.260
10	0.328	0.330	0.331	0.325	0.324	0.329
20	0.382	0.380	0.382	0.376	0.376	0.380
40	0.430	0.429	0.430	0.427	0.429	0.450

6. Vibration and Buckling analysis of column with/without retrofitting

The vibration and buckling performance of thin-walled RC columns, both with and without CFRP retrofitting, was examined under various in-plane partial and concentrated edge loading conditions. Key parameters considered in the analysis include loading position (expressed as the c/b ratio), column height, boundary constraints, and the level at which restraints are applied. A symmetric 4-layer CFRP laminate with a total thickness of 2 mm (stacked in a $(\pm\theta)_S$ configuration) was applied to all column faces for retrofitted cases. The applied load was maintained at a constant intensity of P = 1000 N for both partial and concentrated loading scenarios. For modeling purposes, the column was assumed to have M25-grade concrete with dimensions: height (h) = 3000 mm, width (b) = 1000 mm, and wall thickness (t) = 150 mm.

6.1 Effect of Load Position Ratio and Ply Orientation on Buckling Behavior.

Figures 4(a) and 4(b) illustrate the buckling behavior of a fixed-fixed (C–C) column retrofitted with 2 mm thick carbon/epoxy laminates, applied with different ply orientations. The partial load width is kept constant at 200 mm, and the load position varies with c/b ratios from 0.1 to 0.5. As shown in Fig. 4(a), the critical buckling load increases as the load position ratio (c/b) increases, reaching its maximum at c/b = 0.5, irrespective of ply orientation. The buckling load is observed to be minimal when c/b = 0.1. In contrast, Fig. 4(b) reveals that the critical buckling load remains relatively constant for different c/b ratios,

independent of ply orientation. Additionally, the buckling load increases with the ply orientation, reaching its peak at $\theta = (\pm 90°)_S$ and decreasing with lower orientations, such as $\theta = (\pm 15°)_S$ or $(\pm 0°)_S$. This behavior is attributed to the fact that fiber contribution to buckling resistance is most prominent at $\theta = (\pm 90°)_S$ and diminishes as the ply orientation decreases.

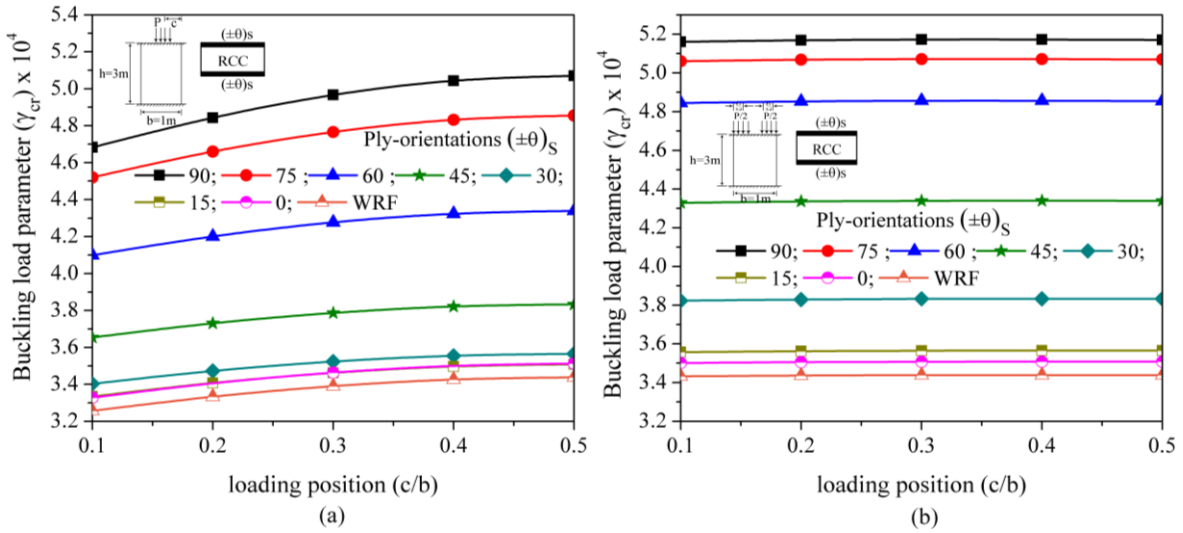

Fig 4: Variation of buckling load (γ_{cr}) with the position of (a) partial load from one edge (b) partial load from both edges.

6.2 Effect of Column Height on Buckling Behaviour.

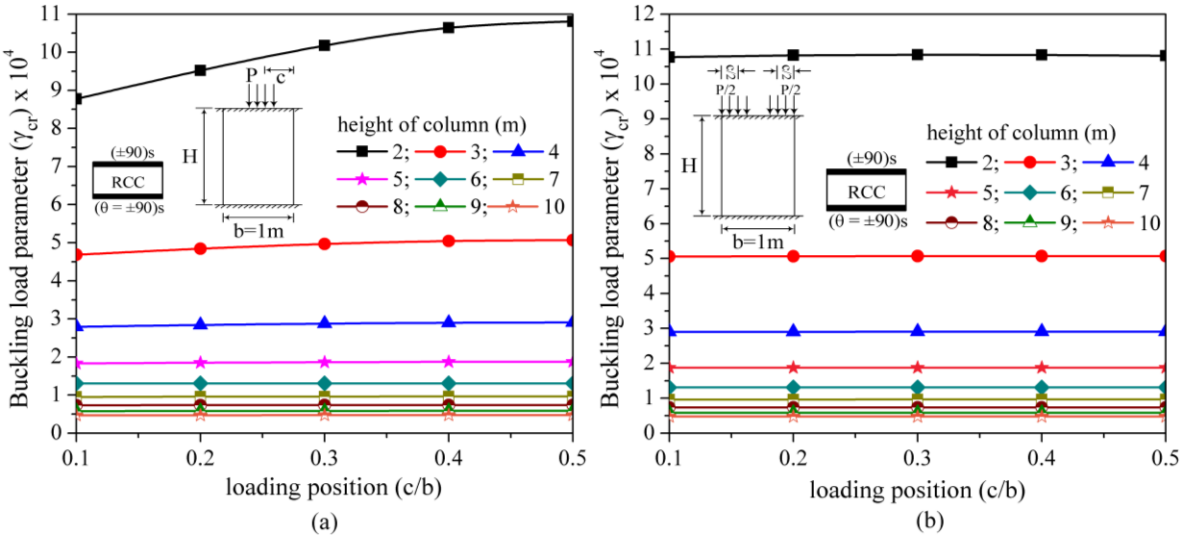

Fig 5: Variation of buckling load (γ_{cr}) for different height (H) with the position of (a) partial load from one edge (b) partial load from both edges .

The effect Figures 5 (a) and 5(b) show the effect of column height on buckling behavior, with the c/b ratio varying from 0.1 to 0.5 and a ply orientation of $\theta = (\pm 90°)_S$. In Fig. 8 (a), the buckling load increases with the c/b ratio, reaching its maximum at c/b = 0.5. The most significant variation is observed for a 2m high column, with a steady decrease in variation as the height increases from 4m to 10m. Notably, for column heights from 7m to 10m, the buckling load remains almost constant.

A dramatic 90% reduction in buckling load is seen as the height increases beyond 7m. In Fig. 5 (b), where the column is subjected to partial load from both edges, the buckling load variation is similar to Fig. 5(a), but the c/b ratio shows little effect across all heights. As column height increases, the stress distribution shifts, becoming more concentrated at the center for shorter columns. The decrease in stress concentration as the column height increases leads to reduced stiffness, which in turn lowers the buckling load.

6.3 Effect of Constraint Position and Partial Edge Load on Buckling Behavior

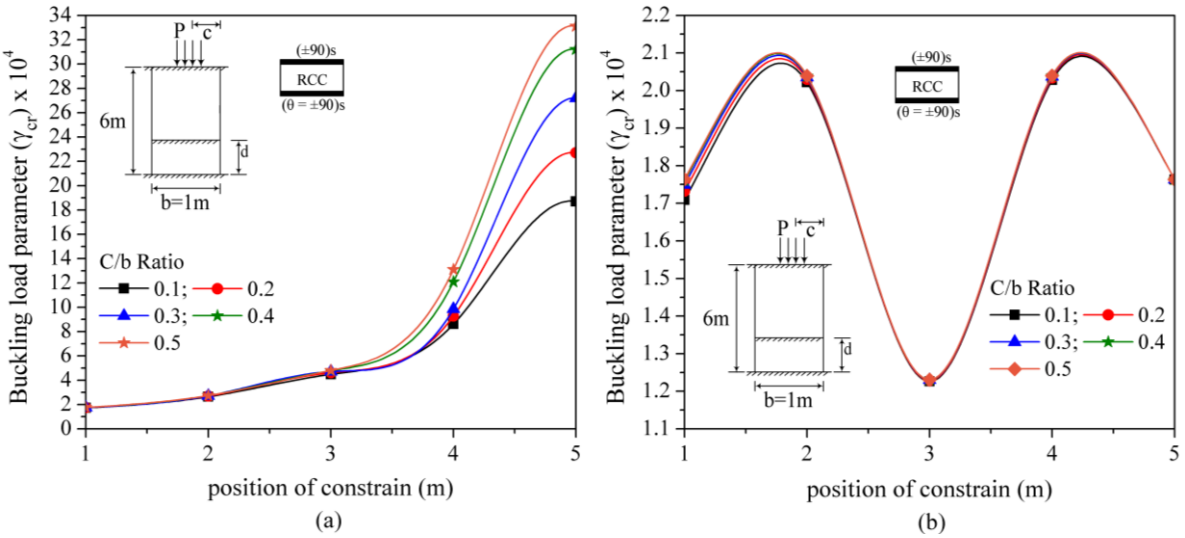

Fig 6: Variation of buckling load (γ_{cr}) for different position of constraint when(a) BC-1 is adopted (b) BC-2 is adopted for intermediate support

Figures 6 (a) and 6 (b) investigate the effect of constraint position on buckling behavior for a 6m high column with partial edge load, varying the c/b ratio from 0.1 to 0.5. In Fig. 6 (a), where all degrees of freedom (d.o.f.) are restrained, the buckling load increases as the constraint moves from 1m to 5m, with the maximum buckling load observed at 5m and c/b = 0.5. In Fig. 9 (b), where only the vertical and lateral d.o.f. are free, the buckling load is highest at 2m and 4m constraint positions, and lowest at 3m, as stress concentration is more evenly distributed. The buckling load at 2m and 4m increases by 18.09%, while at 3m, it decreases by 28.25%.

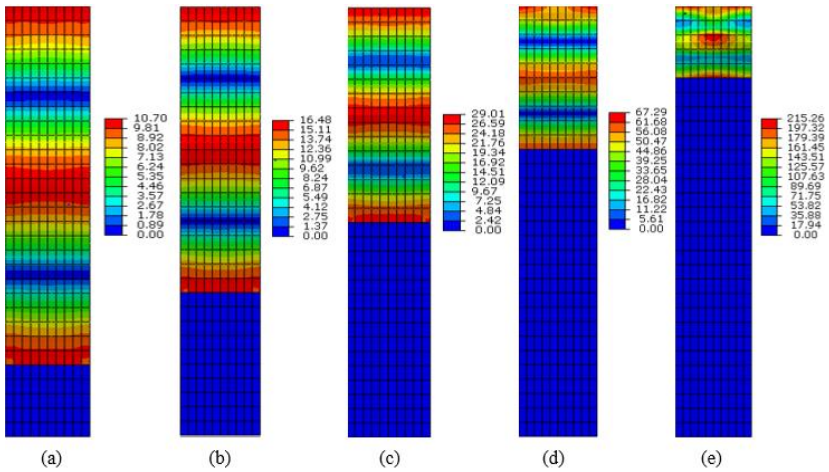

Fig. 7: Stress distributiom for partial load from one edge at c/b = 0.5forBC-1 at intermidate support: (a) 1m, (b) 2m, (c) 3m, (d) 4m, (e) 5m.

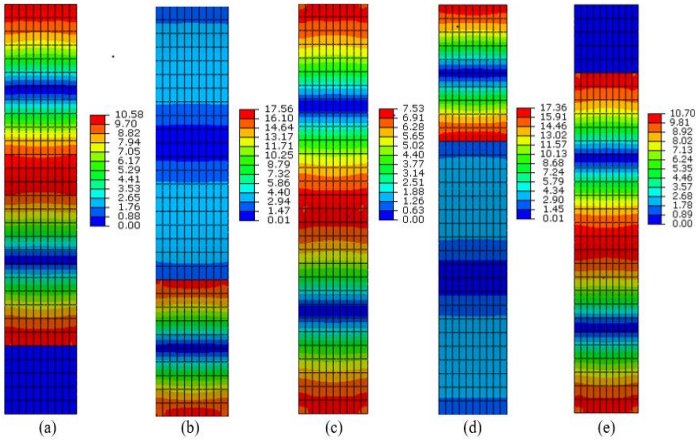

Fig. 8: Stress distributiom for partial load from one edge at c/b = 0.5for BC-2 at intermidate support: (a) 1m, (b) 2m, (c) 3m, (d) 4m, (e) 5m.

Figure 7 shows stress distribution for BC-1, where as the constraint position shifts from 1m to 5m, stress concentration decreases but intensity increases due to the restriction of all d.o.f. In contrast, Fig. 8 illustrates BC-2, where stress is more evenly distributed, with higher concentration near the constraint positions. The study helps identify optimal constraint positions for additional strength, highlighting how restraining d.o.f. affects stress distribution and buckling load. At 5m constraint, buckling load increases by 95.5% for a c/b ratio of 0.5, indicating the critical role of constraint positioning in improving column stability.

6.4 Effect of Storey Number on Buckling Behavior under Partial Load.

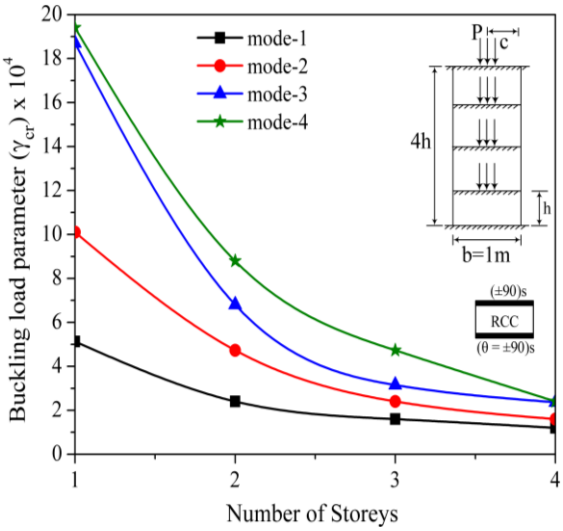

Fig 9: Variation of buckling load (γ_{cr}) for number of storeys with the position of partial load at c/b = 0.5

Figure 9 illustrates the effect of storey number on the buckling behavior of a clamped column subjected to partial edge load with a c/b ratio of 0.5. The results show a significant decrease in buckling load as the number of storeys increases. For a 6m column with 2 storeys, the buckling load reduces by 53.06%, with the reduction becoming less pronounced as the column height or number of storeys increases. The variation in buckling load across different modes in a four-storey column is minimal, as shown in the figure. Mode shapes for two-storey and four-storey columns under partial load with a c/b ratio of 0.5 are presented in Figures 10 and 11.

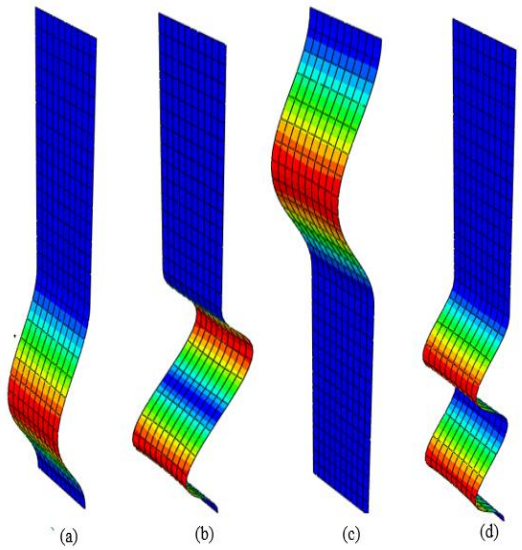

Fig. 10:Critical Mode shapes for two storey with a position of partial edge load edge at c/b = 0.5: (a) mode -1, (a) mode -2, (a) mode -3, (a) mode -4.

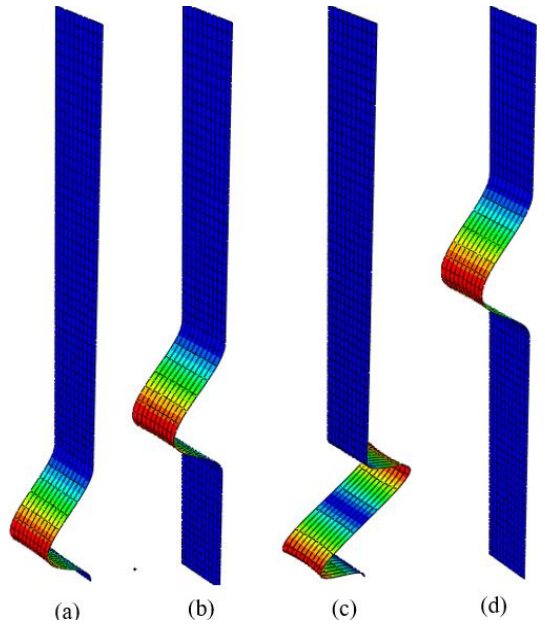

Fig. 11: Critical Mode shapes for four storey with a position of partial edge load edge at c/b = 0.5: (a) mode -1, (a) mode -2, (a) mode -3, (a) mode -4.

6.5 Effect of Boundary Condition on Buckling Behavior of Retrofitted Columns

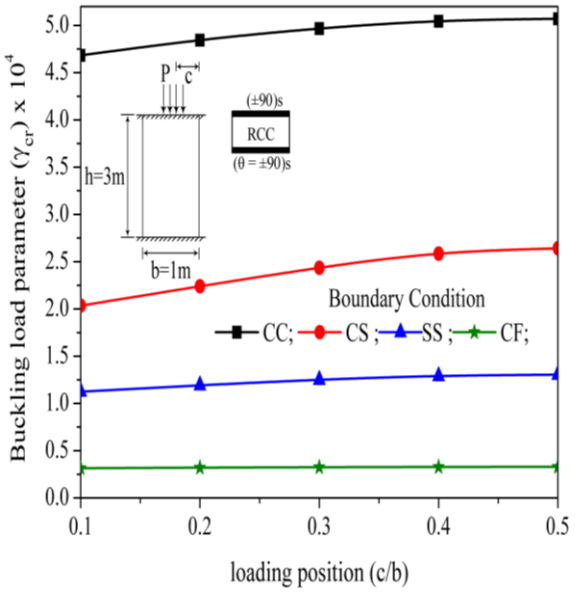

Fig 12: Variation of buckling load (γ_{cr}) for different boundary condition with partial load from one edge c/b = 0.1 to 0.5.

The effect of boundary conditions on the buckling behavior of a column retrofitted with a laminate of ply-orientation θ = (±90°)s and a 2mm thick laminate on each face, subjected to partial load with varying c/b ratios (0.1 to 0.5), is investigated under three different boundary conditions, as shown in Fig. 12. The results reveal that the critical load variation with the c/b ratio is most pronounced for the C-C edged column, while the C-S and S-S edged columns show similar behavior with significant buckling variation across the load width ratios.

7. Vibration Analysis of Retrofitted Concrete Columns.

The vibration analysis of a concrete column retrofitted with carbon/epoxy laminates applied to each face is conducted, considering the effects of various parameters, such as laminate thickness variation, different ply orientations, changes in steel percentage, variations in the breadth-to-thickness ratio, and different boundary conditions. Unless otherwise specified, the laminate stacking sequence is symmetric, with a laminate thickness of 2mm on each face, and the column is rectangular in shape. The column's top and bottom edges are always clamped, except in cases where boundary conditions are specifically studied.

7.1Effect of Laminate Thickness on Vibration Behavior.

This section examines the effect of different laminate thicknesses on the vibration behavior of columns with various ply orientations, as shown in Fig. 13. The results indicate that the natural frequency of the column increases with laminate thickness, regardless of ply orientation, except for ply orientations of θ ≤ (±30°)s, where the increase in natural frequency is minimal. Additionally, the increase in natural frequency is more pronounced when the column is retrofitted with (±90°)s ply orientation compared to the $(\pm 0°)_s$ ply orientation. This can be attributed to the fact that the increase in natural frequency primarily depends on the column's stiffness, which is significantly influenced by fiber orientation. The contribution to stiffness is more pronounced when the laminate is oriented with $(\pm 90°)_s$ fibers, while it is negligible at $(\pm 0°)_s$ fibers.

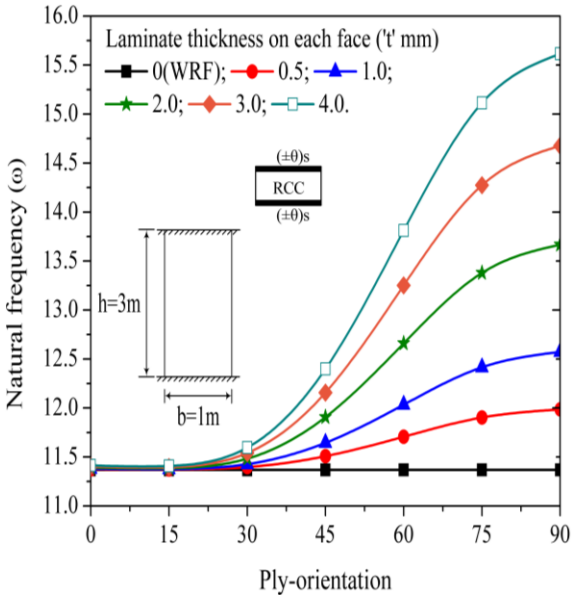

Fig 13: Variation of natural frequency (ω) for different orientation for varying laminate thickness

7.2 Effect of In-Plane Load on Vibration Behavior of Retrofitted C-C Thin- Walled Slender Column

The influence of in-plane load on the vibration behavior of a C-C thin-walled slender column retrofitted with laminate is examined in Fig. 14, considering varying loading positions from a c/b ratio of 0.1 to 0.5.

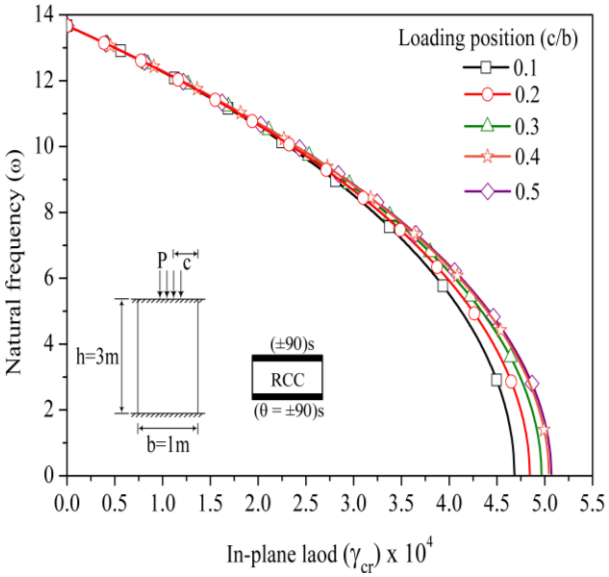

Fig 14: Variation of natural frequency (ω) with load for different loading position

The study is conducted for θ = $(\pm 90°)_s$ with a laminate thickness of 2mm on each face of the column. The results reveal that the frequency at zero load corresponds to the fundamental frequency. As the intensity of the edge load increases, the frequency decreases, regardless of the loading position. Furthermore, the natural frequency of the column decreases and eventually becomes zero at the buckling load, which is the point where the frequency vanishes. This approach helps overcome the limitations of static methods in evaluating critical loads, especially when in-plane stress distribution needs to be considered.

7.3 Variation of Natural Frequency with Ply-orientation and Partial Edge Load

Fig. 15 illustrates the change in natural frequency for a four-layered symmetric laminated column (ply-orientation ranging from θ = $(\pm 0°)_s$ to θ = $(\pm 90°)_s$) subjected to partial edge load with a c/b ratio of 0.5. The results show that at zero loading, the natural frequency increases as the ply-orientation shifts from θ = $(\pm 0°)_s$ to θ = $(\pm 90°)_s$. However, as the load approaches the critical value, the vibrational frequency decreases and eventually becomes zero, regardless of the ply-orientation. It is also noted that the natural frequency is highest at θ = $(\pm 90°)_S$ and lowest at θ = $(\pm 0°)_S$ or θ = $(\pm 15°)_S$, irrespective of the load position. This behavior can be attributed to the fact that the fiber contribution to the natural frequency is most significant when θ = $(\pm 90°)_S$, and it diminishes as the ply-orientation decreases, becoming almost negligible at θ = $(\pm 0°)_S$. These observations align with the results in Fig. 15, supporting the same conclusions.

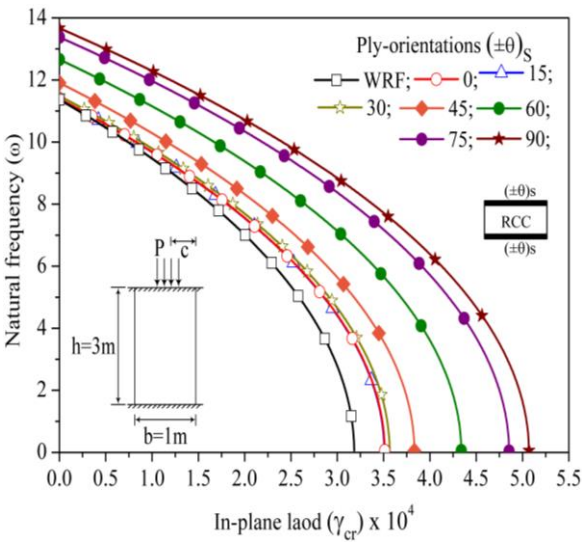

Fig 15: Variation of natural frequency (ω) with load for different ply-orientation.

8. Conclusions

The results from the analysis of slender thin walled column on buckling and vibration behaviour with retrofitting subjected to partial and concentrated edge loading in the plane can be summarized as follows:

1. The buckling load of retrofitted columns is highly influenced by ply-orientation, with the highest buckling resistance observed at $\theta = (\pm 90°)_S$. As the ply-orientation decreases, the column's buckling load reduces due to a decrease in fiber contribution to structural stiffness.

2. The buckling load increases with the increase in load position ratio (c/b), particularly up to c/b = 0.5. However, for columns subjected to partial edge loading, the critical buckling load does not show significant variation for higher values of c/b, especially in columns with complex boundary conditions.

3. The boundary condition plays a crucial role in the stress distribution and buckling behavior. The clamping of degrees of freedom (DOF) increases the stress concentration near the constraint, thereby enhancing the buckling resistance when compared to free DOF at the constraint positions.

4. Column height significantly influences the buckling load, with a considerable reduction in buckling resistance observed as the column height increases. However, beyond a certain height (e.g., 7 meters), the variation in buckling load becomes negligible, indicating a stabilizing effect of increased height.

5. The natural frequency of retrofitted columns increases with the thickness of the laminate and changes in ply-orientation, particularly for $(\pm 90°)_S$ orientations. The natural frequency decreases with applied load, reaching zero at the critical buckling load.

6. The vibration response can provide valuable insights into the critical load conditions, complementing static approaches by considering the in-plane stress distribution. The reduction of the natural frequency to zero at buckling load serves as a reliable indicator of structural failure in slender columns.

References

1. Tayeh, B. A., Maraq, M. A. A., & Ziara, M. M. (2020, December). Flexural performance of reinforced concrete beams strengthened with self-compacting concrete jacketing and steel welded wire mesh. In *Structures* (Vol. 28, pp. 2146-2162).
2. Kaish, A. B. M. A., Jamil, M., Raman, S. N., Zain, M. F. M., & Nahar, L. (2018). Ferrocement composites for strengthening of concrete columns: A review. *Construction and Building Materials*, *160*, 326-340.
3. Deng, M., Zhang, Y., & Li, Q. (2018). Shear strengthening of RC short columns with ECC jacket: Cyclic behavior tests. *Engineering Structures*, *160*, 535-545.
4. M. Khan et al. Khan, M. K. I., Rana, M. M., Zhang, Y. X., & Lee, C. K. (2020).
5. Compressive behaviour of engineered cementitious composites and concrete encased steel composite columns. Journal of Constructional Steel Research, 167, 105967.
6. Saljoughian, A., & Mostofinejad, D. (2016). Axial-flexural interaction in square RC columns confined by intermittent CFRP wraps. Composites Part B: Engineering, 89, 85-95.
7. Shaikh, F. U. A., & Alishahi, R. (2019, August). Behaviour of CFRP wrapped RC square columns under eccentric compressive loading. In Structures (Vol. 20, pp. 309-323). Elsevier.
8. LWang, J., Lu, S., & Yang, J. (2021). Behavior of eccentrically loaded rectangular RC columns wrapped with CFRP jackets under different preloading levels. Journal of Building Engineering, 34, 101943.
9. Isleem, H. F., Peng, F., & Tayeh, B. A. (2022). Confinement model for LRS FRP-confined concrete using conventional regression and artificial neural network techniques. Composite Structures, 279, 114779.
10. Yang, J., Wang, J., & Wang, Z. (2020). Axial compressive behavior of partially CFRP confined seawater sea-sand concrete in circular columns–Part I: Experimental study. Composite Structures, 246, 112373.
11. Smith, S. T., Hu, S., Kim, S. J., & Seracino, R. (2011). FRP-strengthened RC slabs anchored

with FRP anchors. Engineering Structures, 33(4), 1075-1087.
12. Hashemi, S., & Al-Mahaidi, R. (2012). Experimental and finite element analysis of flexural behavior of FRP-strengthened RC beams using cement-based adhesives. Construction and Building Materials, 26(1), 268-273.
13. Wu, Y. F., & Jiang, J. F. (2013). Effective strain of FRP for confined circular concrete columns. Composite Structures, 95, 479-491.
14. Zeng, J. J., Guo, Y. C., Gao, W. Y., Li, J. Z., & Xie, J. H. (2017). Behavior of partially and fully FRP-confined circularized square columns under axial compression. Construction and Building Materials, 152, 319-332.
15. Hadi, M. N. S. (2006). Behaviour of FRP wrapped normal strength concrete columns under eccentric loading. Composite structures, 72(4), 503-511.
16. Belouar, A., Laraba, A., Benzaid, R., & Chikh, N. (2013). Structural performance of square concrete columns wrapped with CFRP sheets. Procedia Engineering, 54, 232-240.
17. Charalambidi, B. G., Rousakis, T. C., & Karabinis, A. I. (2012). Finite element modeling of reinforced concrete columns seismically strengthened through jacketing seismically strengthened through partial FRP jacketing. criterion, 2(1).
18. Hales, T. A., Pantelides, C. P., & Reaveley, L. D. (2017). Analytical buckling model for slender FRP-reinforced concrete columns. Composite Structures, 176, 33-42.
19. Jiang, T., & Teng, J. G. (2012). Theoretical model for slender FRP-confined circular RC columns. Construction and building materials, 32, 66-76.
20. Chellapandian, M., Prakash, S. S., & Rajagopal, A. (2018). Analytical and finite element studies on hybrid FRP strengthened RC column elements under axial and eccentric compression. Composite Structures, 184, 234-248.
21. Mosallam, A., Allam, K., & Salama, M. (2019). Analytical and numerical modeling of RC beam-column joints retrofitted with FRP laminates and hybrid composite connectors. Composite Structures, 214, 486-503.
22. Sahu, S. K., Prabhakar, D. L., & Datta, P. K. (2001). Vibration and buckling of laminated composite plates subjected to non-uniform in-plane edge loading. Journal of Structural Engineering, 28(2), 75-80.
23. Nali, P., & Carrera, E. (2013). Accurate buckling analysis of composite layered plates with combined thermal and mechanical loadings. Journal of Thermal Stresses, 36(1), 1-18.
24. Tseng, Y. P., & Chou, L. C. (1993). Free vibration of orthotropic laminated plates according to partial hybrid plate element. Journal of the Chinese Institute of Engineers, 16(1), 135-143.
25. Kishore, M. H., Singh, B. N., & Pandit, M. K. (2011). Nonlinear static analysis of smart laminated composite plate. Aerospace Science and Technology, 15(3), 224-235.
26. Whitney, J. M., & Riley, M. B. (1966). Elastic properties of fiber reinforced composite materials. Aiaa Journal, 4(9), 1537-1542.
27. Halpin, J. C., & Tsai, S.W. (1969). US Air Force materials laboratory report, AFML-TR. 67.
28. Selvadurai, A. P. S., & Nikopour, H. (2012). Transverse elasticity of a unidirectionally reinforced composite with an irregular fibre arrangement: Experiments, theory and computations. Composite Structures, 94(6), 1973-1981.
29. Hashin, Z., & Rosen, B. W. (1964). The elastic moduli of fiber-reinforced materials. Journal of applied mechanics, 31(2), 223-232.
30. Chamis, C. C. (1989). Mechanics of composite materials: past, present, and future. Composites Technology and Research, 11(1), 3-14.
31. Rajanna, T., Banerjee, S., Desai, Y. M., & Prabhakara, D. L. (2016). Effects of partial edge loading and fibre configuration on vibration and buckling characteristics of stiffened composite plates. Latin American Journal of Solids and Structures, 13, 854-879.